Developmental Biology 375 (2013) 160–171

Contents lists available at SciVerse ScienceDirect

Developmental Biology

journal homepage: www.elsevier.com/locate/developmentalbiology

Sonic hedgehog signaling directly targets *Hyaluronic Acid Synthase 2*, an essential regulator of phalangeal joint patterning

Jiang Liu [a], Qiang Li [b], Michael R. Kuehn [c], Ying Litingtung [a], Steven A. Vokes [b], Chin Chiang [a,*]

[a] Department of Cell and Developmental Biology, Vanderbilt University Medical Center, Nashville, TN 37232, USA
[b] Institute for Cellular and Molecular Biology, The University of Texas at Austin, Austin, TX 78712, USA
[c] Laboratory of Protein Dynamics and Signaling, National Cancer Institute, Frederick, MD 21702, USA

ARTICLE INFO

Article history:
Received 16 October 2012
Received in revised form
28 December 2012
Accepted 29 December 2012
Available online 8 January 2013

Keywords:
Sonic hedgehog
Limb
Joint patterning
Hyaluronic acid synthase
Gli factors
Aggrecan

ABSTRACT

Sonic hedgehog (Shh) signal, mediated by the Gli family of transcription factors, plays an essential role in the growth and patterning of the limb. Through analysis of the early limb bud transcriptome, we identified a posteriorly-enriched gene, *Hyaluronic Acid Synthase 2* (*Has2*), which encodes a key enzyme for the synthesis of hyaluronan (HA), as a direct target of Gli transcriptional regulation during early mouse limb development. *Has2* expression in the limb bud is lost in *Shh* null and expanded anteriorly in *Gli3* mutants. We identified an ~3 kb *Has2* promoter fragment that contains two strong Gli-binding consensus sequences, and mutation of either site abrogated the ability of Gli1 to activate *Has2* promoter in a cell-based assay. Additionally, this promoter fragment is sufficient to direct expression of a reporter gene in the posterior limb mesenchyme. Chromatin immunoprecipitation of DNA-Gli3 protein complexes from limb buds indicated that Gli3 strongly binds to the *Has2* promoter region, suggesting that *Has2* is a direct transcriptional target of the Shh signaling pathway. We also showed that *Has2* conditional mutant ($Has2^{cko}$) hindlimbs display digit-specific patterning defects with longitudinally shifted phalangeal joints and impaired chondrogenesis. $Has2^{cko}$ limbs show less capacity for mesenchymal condensation with mislocalized distributions of chondroitin sulfate proteoglycans (CSPGs), aggrecan and link protein. $Has2^{cko}$ limb phenotype displays striking resemblance to mutants with defective chondroitin sulfation suggesting tight developmental control of HA on CSPG function. Together, our study identifies *Has2* as a novel downstream target of Shh signaling required for joint patterning and chondrogenesis.

Introduction

The Hedgehog family of secreted proteins control growth and patterning during embryogenesis. Sonic hedgehog (Shh) is the most studied vertebrate member and its role has been extensively investigated in the context of limb development. The vertebrate limb originates from the lateral plate mesoderm as a bud-like outgrowth of mesenchymal cells surrounded by an ectodermal layer. Shh expression in the posterior margin of the limb bud defines the zone of polarizing activity, a signaling center that regulates anterior–posterior polarity and distal outgrowth of the limb through a positive feedback interaction with fibroblast growth factor (Fgf) secreted from the apical ectodermal ridge (Niswander et al., 1994; Riddle et al., 1993). This positive loop stabilizes Shh expression, permitting proliferation and survival of mesenchymal precursors that prefigure digit numbers and pattern (Towers et al., 2011; Zhu et al., 2008). Accordingly, the global inactivation of *Shh* leads to truncations of all distal skeletal elements except for a single un-ossified digit 1 (Chiang et al., 2001).

The response to Shh signaling is mediated by three Gli transcription factor family members. Gli1 functions solely as a transcriptional activator whereas Gli2 and Gli3 possess both activator and repressor activities that are regulated by Shh signaling. Genetic studies indicated that Gli1 expression is dependent on Gli2 and Gli3 activator activities (Bai et al., 2004; Motoyama et al., 2003). In contrast, Gli3, and to a limited extent Gli2, are constitutively cleaved into truncated repressor forms while Shh signaling counters this process and converts them to labile activators (Litingtung et al., 2002; Pan et al., 2006; Wang et al., 2000). The loss of Gli3 function leads to polydactyly with defective digit pattern and identity, resembling that of *Shh*;*Gli3* or *Gli2*;*Gli3* double mutants when both repressor and activator activities are abrogated (Bowers et al., 2012; Litingtung et al., 2002; te Welscher et al., 2002). While these observations underscore the importance of Gli activities in the control of limb

* Corresponding author. Fax: +1 615 936 3475.
E-mail address: chin.chiang@vanderbilt.edu (C. Chiang).

0012-1606/$ - see front matter © 2013 Elsevier Inc. All rights reserved.
http://dx.doi.org/10.1016/j.ydbio.2012.12.018

development, much less is known about downstream targets that mediate their functions. Recent genome-wide chromatin immunoprecipitation (ChIP) studies using mouse limb buds derived from transgene expressing an epitope-tagged Gli3 have identified over two hundred putative direct Gli target genes, highlighting the complexity of the regulatory landscape (Vokes et al., 2008).

Using genome-wide microarray analysis of dissected anterior and posterior halves of mouse limb buds, we identified *Hyaluronic acid synthase 2* (*Has2*) as a posteriorly-enriched gene. Although *Has2* is one of three members of the *Has* family, it encodes the enzyme regulating hyaluronan (HA) biosynthesis during mouse embryogenesis as *Has2* null mutants fail to produce HA and die at E9.5-10; in contrast, *Has1* and/or *Has3* null mutants do not exhibit obvious defects, are viable and fertile (Camenisch et al., 2000). HA is a major glycosaminoglycan component of the extracellular matrix, and together with chondroitin sulfate proteoglycans (CSPGs), forms an aggregate network stabilized by link proteins. This supramolecular complex is thought to regulate various cell functions by promoting adhesion, migration, proliferation and signal transduction (Day and Prestwich, 2002; Lee and Spicer, 2000; Toole, 2004; Turley et al., 2002). Embryos in which *Has2* has been conditionally deleted from the limb bud using *Prx1-cre* display partial proximal phalange duplications with defective joints that lack distinct cavities (Matsumoto et al., 2009). However, null mutations that disrupt CSPG function showed earlier, more severe phalangeal patterning defects (Sohaskey et al., 2008; Wilson et al., 2012), suggesting either that the functional complex can still be retained in the absence of HA or that the less severe phenotype in *Has2* conditional knockout represents a partial loss of function.

In this study, we showed that *Has2* expression is dependent on Shh signaling and is ectopically activated in *Gli3* mutant limb buds. Furthermore, we identified two cooperative Gli-binding sites (GBS1 and GBS2) within 3 kb of the *Has2* genomic region, and mutating these sites abolished Gli1-mediated reporter activation in a cell based assay. Chromatin immunoprecipitation of mouse limb buds showed that Gli3 strongly interacts with the region encompassing both GBS1 and GBS2. We also showed that the *Hoxb6-cre* driven *Has2* conditional mutants exhibit severe patterning defects within digits where joints are shifted perpendicularly, closely resembling mutants with defective chondroitin sulfate synthesis or metabolism. Therefore, our findings place *Has2* as an important downstream effector of Shh signaling in the developing limb that is required to establish joint patterning within digits by stabilizing HA-CSPG complexes.

Materials and methods

Gene expression profiling analysis

E10.5 limb buds from 8 litters, with 12–15 embryos per litter, were collected in cold PBS and bisected into anterior and posterior halves. Total RNAs were extracted from anterior and posterior halves using Trizol and purified using a RNeasy Mini kit (Qiagen, CA). Microarray analysis on ~300 μg RNA from each sample was carried out by the Vanderbilt Microarray Core facility using Affymetrix Mouse Exon 1.0 ST Array. The microarray data has been deposited in the Gene Expression Omnibus (GEO) database (GSE41691). RNA samples were also reverse transcribed using iScript cDNA synthesis kit (Bio-Rad, CA) and subjected to RT-PCR using primer sets as follows: *Has2* Forward: 5′-GTCCAAGTGCCTTACTGAAACTCCC-3′; *Has2* Reverse: 5′-GAGGATGTTCCAGATTTTACCCCTG-3′; *Gli1* Forward: 5′-CTGGAGAACCTTAGGCTGGA-3′; *Gli1* Reverse: 5′-CGGCTGACTGTGTAAGCAGA-3′; *Shh* Forward: 5′-TCTGTGATGAACCAGTGGCC-3′; *Shh* Reverse: 5′-GCCACGGAGTTCTCTGCTTT-3′ and *Gapdh* Forward: 5′-TTCACCACCATGGAGAAGGC-3′; *Gapdh* Reverse: 5′-GGCATGGACTGTGGTCATGA-3′.

Animals

The *Has2* conditional targeting construct was generated using the recombineering technique as previously described (Copeland et al., 2001; Liu et al., 2003). Briefly, a genomic region of 9.5 kb, spanning exon 2 of *Has2*, was retrieved from a BAC clone (ID: bMQ-150M3) into a diphthera toxin (DTA)-expressing plasmid by recombineering. A loxp site was then inserted 50 bp upstream of exon 2, followed by the integration of frt-neo-frt-loxp cassette 500 bp downstream of exon 2 via two rounds of recombineering. The resulting *Has2* targeting vector contained 5′ and 3′ homologous arms, two loxp sequences flanking exon 2, a flp recombinase removable neo cassette and the DTA gene (Fig. S1). To generate *Has2* conditional knockout allele, the NotI-linearized targeting vector was electroporated into mouse R1 ES cells (Nagy et al., 1993). Colonies that were negative for DTA and resistant to G418 selection were further screened by Southern blotting after HindIII digestion and analyzed by PCR to identify correctly targeted ES clones (Fig. S1). Targeted ES cells were injected into C57Bl6 blastocysts through the Vanderbilt Transgenic Mouse/Embryonic Stem Cell Shared Resource, and strong chimeras were subsequently backcrossed with Black Swiss mice to obtain germline transmission mice that carried heterozygous *Has2* targeted allele. The *neo* selection cassette was then removed by crossing the heterozygous mice with *flpe* mice expressing flp recombinase (Rodriguez et al., 2000) to generate $Has2^{flox}$ mice. Limb specific deletion of *Has2* was achieved by crossing to the *HoxB6*-cre line (Lowe et al., 2000). $Shh^{-/-}$ and $Gli3^{xt}$ mice were as previously described (Litingtung et al., 2002).

In situ hybridization and immunohistochemistry

Whole mount and section in situ hybridizations were performed using digoxygenin-labeled riboprobes as previously described (Li et al., 2006, 2008). Riboprobes were synthesized using the digoxygenin RNA labeling kit (Roche). The probes used were *Has2* (IMAGE:30533251), *Gdf5* (IMAGE:4190036), *Wnt4* (Gavin et al., 1990), *Chordin* (Klingensmith et al., 1999), *Sox9* (Ng et al., 1997), *Noggin* (McMahon et al., 1998), *Col2a1* (Ng et al., 1997) and *Pgk1*(IMAGE:6828087). Immunohistochemistry on paraffin-embedded sections were performed as previously described (Li et al., 2004). For detection of aggrecan and link protein, tissue sections were first treated with 0.1% trypsin for 10 min at 37 °C for enzymatic antigen retrieval, and then with chondroitinase ABC (0.25 unit/ml; Sigma) for 30 min prior to incubation with the primary antibodies. The primary antibodies were rabbit anti-phosphorylated Erk1/2 (Cell signaling, 1:200), rabbit anti-cleaved Caspase 3 (Cell Signaling, 1:200), rabbit anti-phosphorylated Histone 3 (Millipore, 1:1000), mouse anti-CSPG (DSHB, 9BA12, 1:10), mouse anti-aggrecan (DSHB, 12/21/1-C-6, 1:10) and mouse anti-link protein (DSHB, 9/30/8-A-4, 1:10).

Chromatin immunoprecipitation (ChIP)

The $RosaGli3T^{Flagc/c}$ line, which contains a Cre-inducible 3XFlag-tagged Gli3 repressor (Vokes et al., 2008), was crossed with homozygous *Prx1Cre* mice (Logan et al., 2002). For each ChIP experiment, we collected forelimbs and hindlimbs from a single litter of eight or nine E11.5 embryos and performed ChIP with the M2 anti-Flag monoclonal antibody (Sigma) as described previously (Vokes et al., 2007, 2008), performing a total of three independent experiments. For a negative control, limb buds were dissected from a single litter of E11.5 wildtype Swiss Webster embryos and ChIP was performed using the same anti-Flag antibody. The occupancy of Gli3 repressor on the *Has2* locus was measured by realtime q-PCR using primer sets targeting different

loci of the *Has2* promoter region. q-PCR was performed in 20 μl reaction containing SYBR Green Master Mix (ABI), and ran on the ViiA7 Real-Time PCR System (ABI). The primer sets used were: P1: primer set#1, Forward CTCATGGCAATGGGTTTTCT and Reverse TGCATGATATGCAGTCCACA; P2: primer set#2, Forward AGAGGGGAGAACCAAGCATT and Reverse AGGGTCGTGGAAGGAAGTTT; P3: primer set#3, Forward CAAGGATTCCCTCGACTTGA and Reverse CACGGACGTACACACACACA; P4: primer set#4, Forward GGCTGGACACTGAAATGAGG and Reverse AAGGCTGTCAAGAGGCAAAA; P5: primer set#5, Forward CTTGTGGGCATTTAGGCATT and Reverse TCAGACCTGAGCTTCCTGGT; P6: primer set#6, Forward CATGGAAGCCAGAAGAGGTT and Reverse AGCATGCCAAGATCCTATGC; Gli1 Gli3-ChIP site, Forward GGACAAAGAGACCTGGGACA and Reverse AGGAGATGCTCTGACGCCTA; Ptch1 Gli3-ChIP site, Forward AGGCCTGCACCAATAATGAC and Reverse TCCTTGCTCGCCTCTTTAAC and Baseline, Forward CTGGCCTCCATACACACATA and Reverse AGTCAGCAGGATCCACACTT. The enrichments were calculated by the delta(delta)Ct method and the enrichment levels of each primer set are shown as Log2 values.

Cell-based luciferase reporter assay

The 2880 bp promoter sequence (mm9|chr15:56525549–56528428) of *Has2* was generated by PCR and cloned upstream of the luciferase reporter in pGL3 Basic plasmid (Promega, WI). Primers used were as follows: Forward: ttgtctcgagTATGAATGCATCAACGATAAACG and Reverse: atttaagcttCTTGTTCAGCTCCTGCTCATAGA. Mutations at putative Gli binding sites (M1: GCCCACCCA to GCCagCtgA; M2: GACCACACA to GACagCtgA) were generated using a QuikChange mutagenesis kit (Stratagene, CA). Luciferase assays were performed essentially as previously described (Huang et al., 2010), using the Promega Dual Luciferase Reporter Assay system (Promega, WI). All reporter assays were normalized using Renilla luciferase as internal control. Each data point represents the mean of triplicate wells with error bar representing the standard deviation (SD).

Skeletal staining

Whole-mount skeletal staining with Alcian blue and Alizarin red to visualize cartilage and mineralized bone was performed as described (Chiang et al., 2001).

Micromass culture

Micromass cultures were prepared from E11.5 hindlimbs as previously described (Ahrens et al., 1977; James et al., 2005; Stanton et al., 2004). Dissociated cells were resuspended in growth medium at a concentration of 2×10^7 cells/ml and spotted as 10 μl droplets onto 24-well plates. Cells were allowed to adhere for 2 h at 37 °C, then 500 μl of 1:1 DMEM/F-12 medium containing 10% FBS was added. Growth medium was replaced every other day. At day 7 after seeding, micromass cultures were collected for Alcian blue staining or *Col2a1* micromass whole mount in situ hybridization according to published methods (Cash et al., 1997).

Results

Has2 expression in the posterior limb bud mesenchyme is dependent on signaling Shh

In an effort to identify downstream targets of Shh signaling, we performed microarray analysis on an Affymetrix Exon array using total RNAs extracted from the anterior and posterior halves of E10.5 mouse limb buds (Fig. 1A). We identified *Hyaluronan Acid Synthase 2* (*Has2*), which was upregulated 1.35 fold in the posterior limb, as a candidate gene regulated by Shh signaling. In this screen, other known Shh target genes that were upregulated in the posterior limb include *Ptch1* (2.23 fold) and *Gli1* (1.54 fold). RT-PCR analysis confirmed the enriched posterior expression of *Has2* in developing limb buds, as were *Shh* and *Gli1* (Fig. 1B). RNA in situ hybridization revealed that *Has2* mRNA expression starts as early as E9.5 and its dynamic expression domain expands with limb growth but is restricted posteriorly from E9.5 to E11.5 (Fig. 1C and J), although low level expression in the proximal region adjoining the body wall can be detected (* in Fig. 1C, G and K). *Has2* expression in the hindlimb was consistently lower than that in the forelimb, which is in agreement with the fact that there is ~12 h delay in the development of the hindlimb compared to forelimb. At E12.5, *Has2* expression becomes largely restricted to the condensing digit mesenchyme (Fig. 1O and P). To determine whether *Has2* expression is dependent on Shh signaling, we examined *Has2* mRNA expression in $Shh^{-/-}$ mutants. *Has2* expression is dramatically reduced in $Shh^{-/-}$ mutant limb buds at E10.5 (Fig. 1M and N) and E11 (Fig. 1Q and R) whereas its most proximal expression abutting the body wall remains (* in Fig. 1M and Q). Similarly, at E12.5 *Has2* expression in the distal limb is largely absent but low level expression persists in the proximal region of the autopod (Fig. 1Y and Z). These observations strongly suggest that *Has2* expression depends on Shh signaling.

Has2 expression in the anterior limb bud is suppressed by Gli3 repressor

The patterning function of Shh is mainly mediated by Gli3 in the limb. In the presence of Shh signaling, the full-length form of Gli3 protein (Gli3-FL) is activated and functions as a transcriptional activator (Gli3A). In the absence of Shh signal, as in the anterior limb bud, Gli3-FL is cleaved into a repressor form (Gli3R) where it suppresses the expression of Shh-responsive genes (Litingtung et al., 2002; te Welscher et al., 2002). By examining *Has2* mRNA expression in $Gli3^{xt}$ mutants, which lack Gli3 function, we identified an ectopic expression domain in the anterior margin of the limb underlying the AER (Fig. 1S and T, arrows), indicating that Gli3R represses *Has2* expression in the anterior limb. This ectopic *Has2* expression persisted *in* $Shh^{-/-}$;$Gli3^{xt}$ double mutants (Fig. 1U and V, arrows), suggesting that activation of anterior *Has2* expression does not require Shh pathway activation and can be activated by Gli3R derepression. However, the posterior expression of *Has2* in $Shh^{-/-}$; $Gli3^{xt}$ double mutant limbs was reduced, suggesting a GliA contributes quantitatively to normal expression levels (Fig. 1U and V). Together, these data suggest that Gli activators are likely to play a role, in addition to Gli3R, in regulating *Has2* expression in the limb.

Has2 is a direct target of Gli transcription factors

Based on our genetic data, we hypothesized that Shh signaling directly regulates *Has2* expression in early limb development. The Gli transcription factors are Shh signaling effectors and have DNA binding zinc finger domains to bind to the consensus sequence TGGGTGGTC on target genes to initiate or suppress transcription (Hallikas et al., 2006; Kinzler and Vogelstein, 1990; Vokes et al., 2007, 2008; Vortkamp et al., 1995). Through *in silico* analysis, we identified two such consensus sequences within the 3 kb *Has2* regulatory region, one at −646 bp (Gli-binding site 1,GBS1) and the other at +504 bp (GBS2) from the *Has2* transcriptional start site (+1) (Fig. 2A and B).

To determine if these binding sites are capable of responding to Gli1 activation, we generated *Has2* reporter constructs by cloning

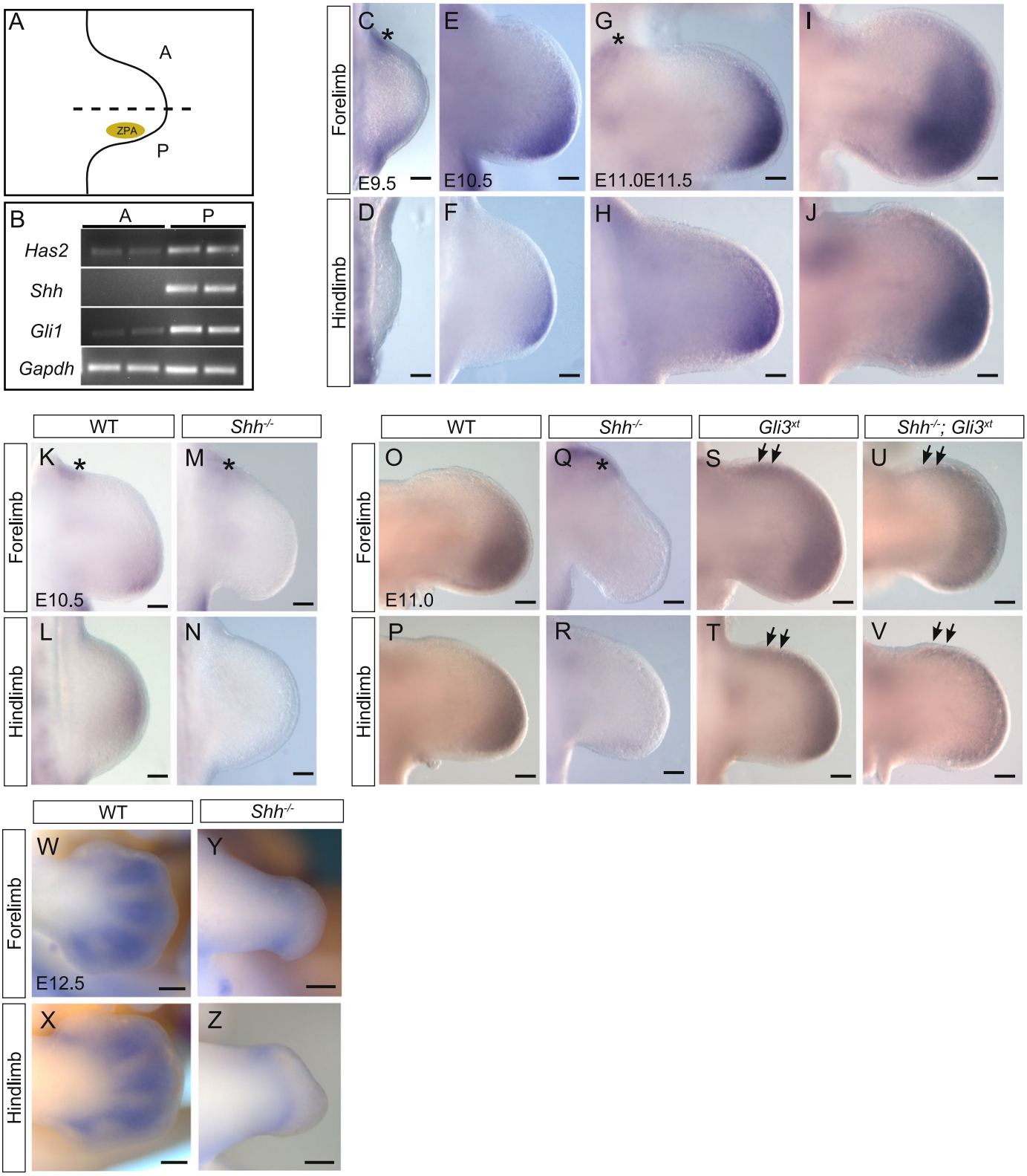

Fig. 1. *Has2* is regulated by Shh signaling in the limb bud. (A) E10.5 limb illustration with posterior domain (P), anterior domain (A) and the Zone of polarizing activity (ZPA). For anterior versus posterior tissue analysis, the limb was bisected at the midline (dotted line). (B) RT-PCR of anterior and posterior halves of limb buds showing increased expression of *Shh*, *Gli1* and *Has2* in the posterior domain. *Has2* expression in mesenchyme of forelimb (C, E, G and I) and hindlimb buds (D, F, H and J) from E9.5 to E11.5 by whole mount RNA in situ hybridization. Posterior *Has2* expression is undetectable in E10.5 $Shh^{-/-}$ (M and N) compared with WT (K and L) limb buds. At E11, posterior *Has2* expression is barely detectable in $Shh^{-/-}$ (Q and R) compared with WT (O and P) limb buds. *Has2* expression is expanded anteriorly in $Gli3^{xt}$ mutant limb buds at E11 (S and T, arrows) compared with wildtype (O and P). Note diminished *Has2* mRNA in posterior limbs of $Shh^{-/-}$;$Gli3^{xt}$ double mutants while expanded anterior *Has2* remains comparable to $Gli3^{xt}$ limbs (U and V, arrows). Low level *Has2* expression in the most proximal region adjoining the body wall can be detected in WT (C, G, K and *) and this expression is unaltered in $Shh^{-/-}$ (M, Q and *). (W–Z) At E12.5, *Has2* expression is mostly confined to the condensing digit mesenchyme (W and X), and this patterns of expression is largely absent in Shh mutants although low level *Has2* expression persists in the proximal region of the autopod (Y and Z). Scale bar, 75 μm.

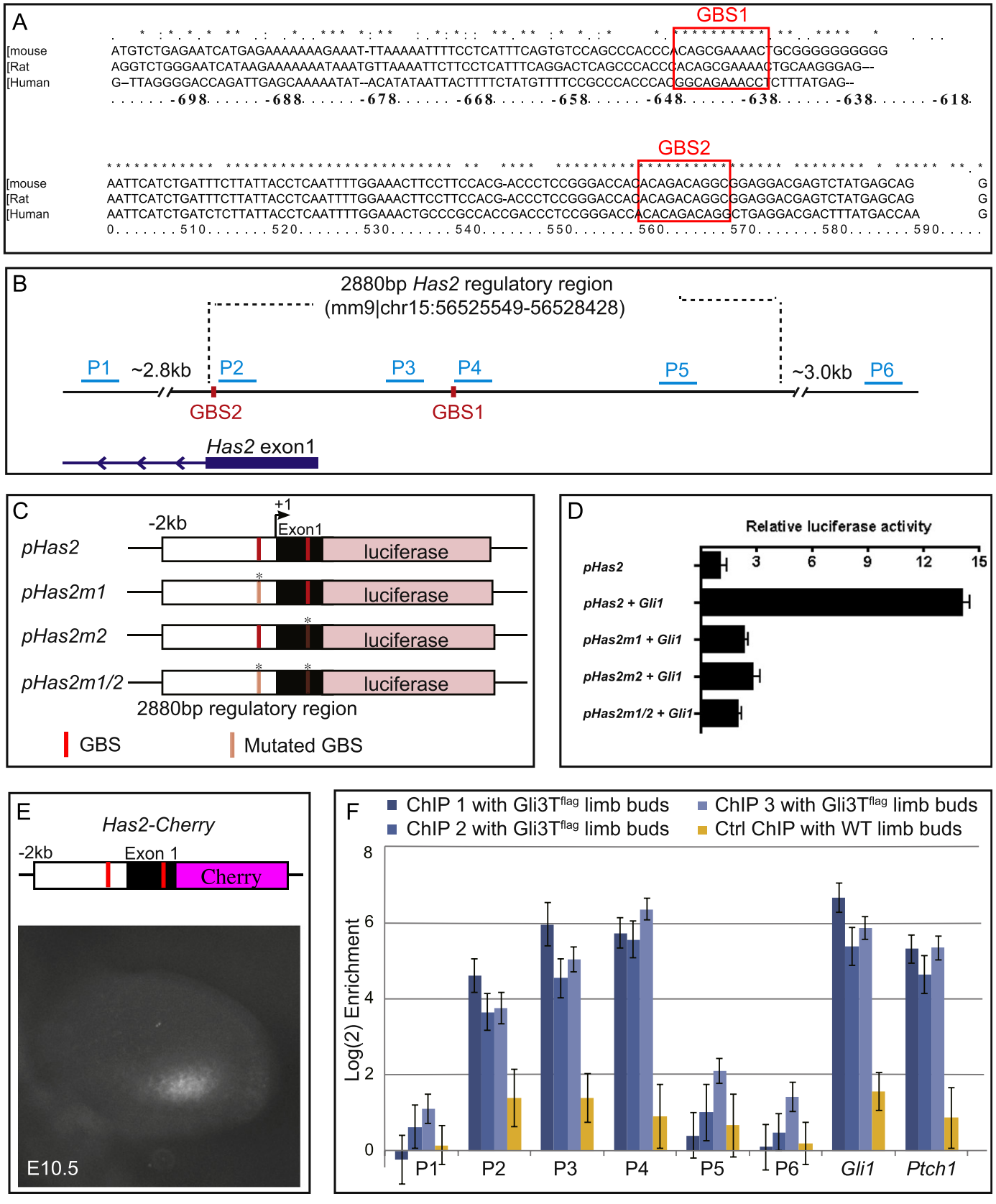

Fig. 2. Gli transcription factors directly regulate *Has2* promoter activity. (A) Prediction *in silico* identified two potential Gli-binding sites, which are highly conserved in mammals, in the *Has2* promoter. (B) Illustration of genomic *Has2* regulatory region; ~3.0 kb *Has2* regulatory region was used for luciferase assays. P1 through P6 were target sequences used to identify in vivo Gli binding by chromatin immunoprecipitation (ChIP). Note that the 5′ untranslated region (5′ UTR) spans exon 1 of *Has2*. (C) Reporter constructs used in luciferase assays. ~3.0 kb *Has2* regulatory region was subcloned into pGL3 luciferase plasmid (*pHas2*). Potential Gli binding motif was singly mutated (*pHas2m1*, *pHas2m2*) or doubly mutated (*pHas2m1/2*). (D) Normalized luciferase values obtained when 3T3 cells were cotransfected with various derivatives of *Has2* luciferase reporter with or without *Gli1* expression construct. (E) ~3 kb *Has2* promoter is sufficient to direct Cherry reporter expression in the posterior limb mesenchyme. (F) *FlagGli3* ChIP for in vivo detection of Gli3 binding to *Has2* promoter. Regions spanning the two potential Gli binding motifs (P2–P4) are substantially enriched by 30–60 folds, similar to enrichment for positive control loci *Gli1* and *Ptch1*. The positive control regions are validated Gli3 binding regions near the *Gli1* and *Ptch1* loci (Vokes et al., 2008). ChIP1, ChIP2 and ChIP3 represent three independent biological samples of anti-Flag ChIP using E11.5 *Prx1Cre*; *RosaGli3T*$^{Flagc/c}$ limb buds. Ctrl ChIP represents same stage wildtype limb buds. All assays were performed in triplicate and error bars represent the standard error of mean.

the ~3 kb *Has2* promoter fragment upstream of the luciferase gene (Fig. 2B and C). The *Has2* reporter, either unaltered or containing mutation at one or both GBSs (Fig. 2C), was then co-transfected with *Gli1*-expressing or control vector into Shh-responsive 3T3 cells (Taipale et al., 2000). Consistent with the presence of GBSs, we observed significant induction of luciferase activity by Gli1 (Fig. 2D). Importantly, mutations in either or both GBSs reduced reporter activity to basal level, indicating that these sites are necessary for Gli1 activation and may function cooperatively (Fig. 2D).

We next performed transgenic analysis to further characterize the *Has2* promoter fragment and found that it contains the necessary cis-regulatory elements to direct expression of a reporter gene in the posterior limb mesenchyme (Fig. 2E), revealing the relevance of this region in the context of limb development and Shh regulation.

To determine whether Gli can directly bind to GBSs at the *Has2* promoter region in vivo, we utilized *Prx1-cre*; *RosaGli3T*$^{Flagc/c}$ transgenic embryos in which FLAG-tagged Gli3 repressor is expressed under the control of ubiquitous *Rosa26* promoter which is selectively activated in the early limb mesenchyme by *Prx1-cre* (Vokes et al., 2008). We designed several q-PCR primer sets within the *Has2* regulatory region, P1 through P6 (Fig. 2B), and performed ChIP using antibody against the FLAG epitope followed by q-PCR analysis on Gli3-bound chromatin to determine enrichment of PCR products. Regions spanning the two GBSs (P2–P4) were enriched by 30–60 folds, similar to enrichment for known Gli target genes *Gli1* and *Ptch1* (Fig. 2F). In contrast, regions tested that were outside the GBSs either ~2.8 kb upstream (P1) or 3.0 kb downstream (P6) showed no enrichment, indicating that Gli binds directly to this regulatory region of *Has2* in vivo (Fig. 2F). This is consistent with Gli3T binding observed at this site in a previously published genomic dataset (Vokes et al., 2008).

Has2 conditional mutants display mispatterning of joints and defective chondrogenesis

To elucidate the role of Shh-induced *Has2* in early limb development, we generated a *Has2* conditional knockout allele (*Has2*^{fl}) to circumvent the early lethality of *Has2* null mutants (Camenisch et al., 2000) (Fig. S1). We selected *Hoxb6-cre* to inactivate *Has2* function in the early limb mesenchyme based on the observations that *Hoxb6-cre* is more effective than *Prx1-cre* in abrogating gene function in early limb buds when crossed to various conditional mutants (Li et al., 2005; Lowe et al., 2000; Scherz et al., 2007; Yu and Ornitz, 2008; Zhu et al., 2008). Because the rostral limit of *Hoxb6* expression domain is confined to the posterior forelimb, all analyses were performed in hindlimbs except where noted. Indeed, skeletal preparation of newborn *Hoxb6Cre*;*Has2*$^{fl/-}$ (hereinafter referred to as *Has2*^{cko}) hindlimbs showed much more severe phenotype than previously described (Fig. 3A and B) (Matsumoto et al., 2009). Focusing on the digits, the mutants displayed longitudinally oriented cavities that split proximal and medial phalanges (Fig. 3E, E′ versus F, F′). As expected, the digit defect in the forelimb is restricted to the posterior digits (Fig. 3C and D). Histological staining at E16.5 showed that the space adjoining the split phalanges is occupied by distinct loosely associated mesenchymal cells that are reminiscent of cells at interphalangeal joints (Fig. 3 G, G′ versus H, H′). Additionally, the mutant digits displayed disorganized cartilage nodules, suggesting a role of *Has2* in chondrogenesis (Fig. 3F, F′, H, H′). Consistent with this finding, limb micromass cultures of *Has2*^{cko} followed by Alcian blue staining or *Col2a1* (type II collagen) expression revealed striking loss of cartilage-forming potential (Fig. 3I, J and K, L).

The first histological indication of synovial joint formation is the appearance of flattened cells at a stereotypic joint location known as the interzone at ~E12.5 in mouse digits. As development proceeds, the interzone undergoes cavitation, a process where physical separation of opposing skeletal elements occurs (Khan et al., 2007). While the mechanism involved in joint forming activities remains to be fully deciphered, both programmed cell death and Erk activation have been implicated in this process (Fernandez-Teran et al., 2006; Pitsillides, 2003; Pitsillides and Ashhurst, 2008; Seo and Serra, 2007). Because *Has2*^{cko} mutants displayed perpendicularly oriented joint cavities in the digits, we sought to determine whether there was a similar shift in the expression pattern of pErk and cleaved Caspase 3 for cell death. At E14.5, p-Erk (Fig. 3M and M′) and cleaved Caspase-3 (Fig. 3O and O′) immunoreactivities are normally restricted to the joint perpendicular to the digit shafts but these expressions were mislocalized along the longitudinal axis in *Has2*^{cko} mutant digits (Fig. 3N, N′, P and P′). Therefore, the disruption of *Has2* function leads to ectopic joints along the digit rays.

Has2 is required for positioning the interzone

To evaluate the effect of *Has2* deficiency on joint development in detail, we examined the expression of *Gdf5*, an early joint-specific marker (Koyama et al., 2008; Storm and Kingsley, 1996). *Gdf5* expression in the autopod is first detectable at ~E12 in the perichondrium bordering the condensing digit rays (Storm and Kingsley, 1996) (Fig. S2). As development proceeds, perichondrial *Gdf5* expression diminishes while interzone expression becomes more prominent (Fig. 4A, C and E). In *Has2*^{cko} mutants, however, we observed much broader expression of *Gdf5* in the interzone at E12.5 (Fig. 4B) although perichondrial expression is initiated normally (Fig. S2). By E13, the aberrant *Gdf5* expression became more pronounced, as evidenced by longitudinal stripes of presumptive joint progenitors bisecting the proximal/medial phalanges and this pattern persisted throughout joint development (Fig. 4D and F).

The expression of other joint markers such as *Wnt4* (Fig. 4O and P) and *Chordin* (Fig. 4Q and R), were also altered in *Has2*^{cko} mutant hindlimbs as highlighted by longitudinal shift in their expression pattern when compared to control. *Noggin* expression in condensing cartilage also highlights the misplacement of phalangeal joints at E14.5 in *Has2*^{cko} hindlimbs (Fig. 4N) compared with wildtype showing clear demarcation of the joint region (Fig. 4M). Likewise, *Sox9* expression from E12.5 to E13.5 in condensing cartilage mesenchyme highlights aberrant joint formation and longitudinal shift in *Has2*^{cko} (Fig. 4H, J and L) compared with wildtype joints (Fig. 4G, I and K; arrows showing normal joint location). We note that *Sox9* expression in digit rays in hindlimb buds of WT and *Has2*^{cko} at E12 were comparable suggesting that commitment of mesenchymal cells to the chondrocytic lineage was not affected by loss of *Has2* expression (Fig. S2). We also determined the status of cell proliferation using mitotic marker phosphorylated-Histone 3 in E12.5 and E13.5 hindlimbs (Fig. S3). We did not find significant alteration in cell proliferation at these stages compared to wildtype when joint defects were already apparent in *Has2*^{cko} limb buds.

Disruption of CSPG-link protein-hyaluronan aggregates and impaired phalangeal mesenchymal condensation in Has2^{cko}

The profound joint patterning defects observed in our *Has2* conditional mutants are strikingly similar to mouse mutants that are either deficient in CSPG or imbalanced in proteoglycan sulfation (Sohaskey et al., 2008; Wilson et al., 2012). We therefore examined whether CSPG development is affected in *Has2*^{cko}. At pH 2.5, Alcian blue stains most acidic proteoglycans, while at pH1 only sulfated proteoglycans are stained (Lev and Spicer, 1964). We observed remarkable loss of Alcian blue pH1 staining in the

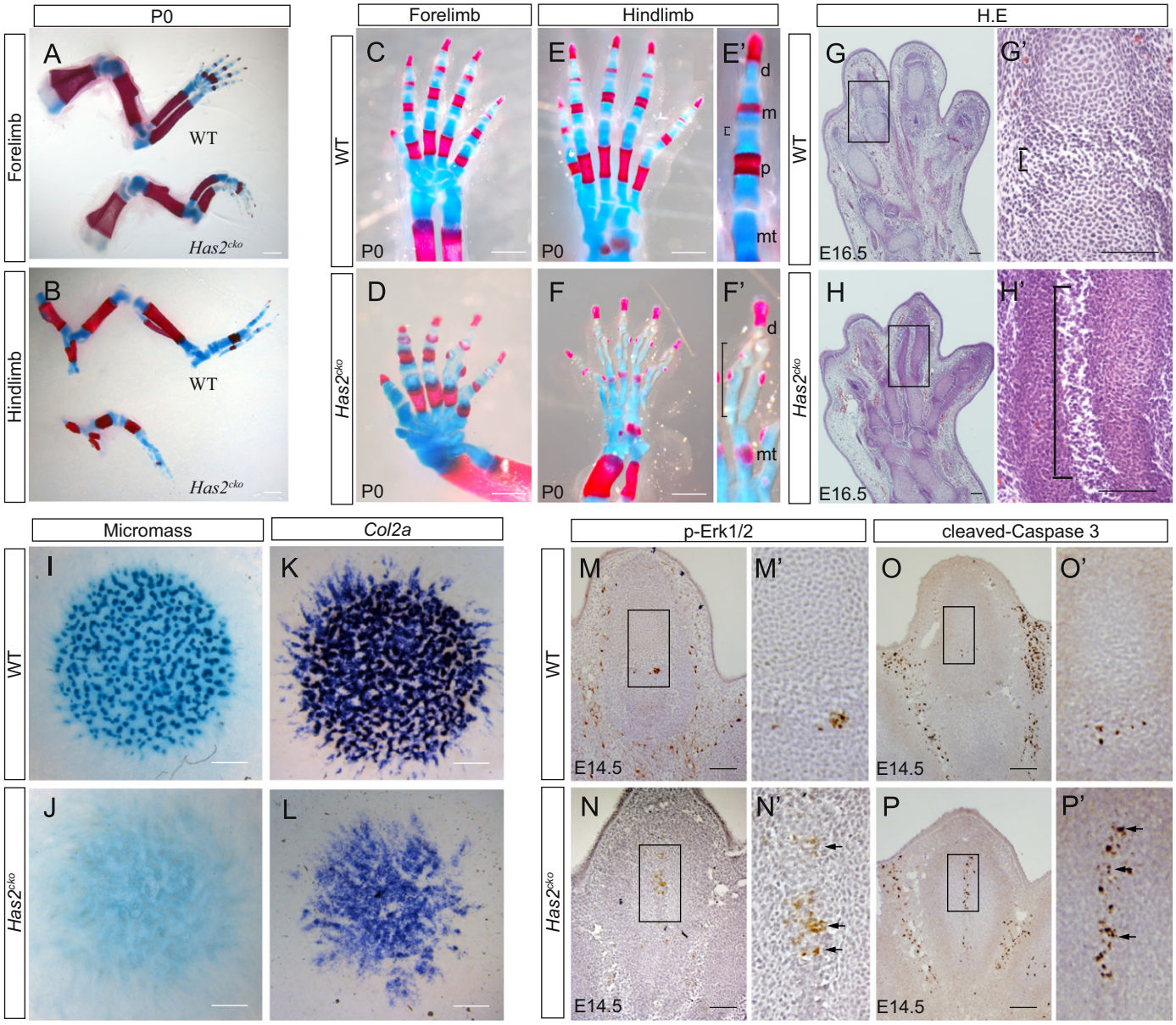

Fig. 3. *Has2*^{cko} mutant hindlimbs display chondrogenesis and joint positioning defects. Whole-mount skeletal elements of P0 wild-type and *Has2*^{cko} forelimbs (A) and hindlimbs (B) stained with Alizarin red and Alcian blue. Severe cartilage reduction and joint positioning defect are apparent in P0 *Has2*^{cko} digits (D, F, F') when compared to wildtype (C, E, E'); note that interphalangeal joints highlighted by brackets are perpendicularly shifted in *Has2*^{cko} mutants. Hematoxylin and Eosin staining of E16.5 hindlimb sections (G and H), with higher magnification view of joint cavities (G′ and H′). In addition to aberrant joint formation, the mutants (H and H′) also show prominent change in phalangeal cartilage nodule organization indicating defective chondrogenesis. *Has2*^{cko} limb micromasses J and L) show reduced chondrocyte differentiation while wildtype (I and K) display robust capacity to differentiate as shown with Alcian blue staining (I and J) and *Col2a* expression (K and L). Sections of E14.5 digits immunostained with p-Erk1/2 (M and N) and cleaved-Caspase 3 (O and P) showing ectopically expanded expression of p-Erk in *Has2*^{cko} digits (N′, arrows) and likewise cleaved Caspase 3 is also expanded (P′, arrows). Note that this orthogonally shifted pattern in *Has2*^{cko} agrees with the ectopic positioning of *Gdf5*-expressing joint cells (G′ versus H′). In contrast, wildtype littermates show p-Erk (M and M′) and cleaved Caspase 3 (O and O′) expressions confined to cells in the normal joint interzone (M′ and O′). Scale bar, 500 μm (white) and 50 μm (black).

Has2^{cko} condensing digit rays while the interdigital mesenchyme acquired Alcian blue staining at E12.5 (Fig. 5B and C, arrows), suggesting loss of CSPG integrity and its aberrant distribution in *Has2*^{cko} hindlimbs. Note that in the wildtype, Alcian blue staining is strong and confined to digits, with no apparent staining in the interdigital space (Fig. 5B, arrows). Similarly, CSPG immunostaining was strongly reduced in *Has2*^{cko} condensing digits when compared to control digits (Fig. 5E versus D). Moreover, we observed striking CSPG labeling in the interdigital mesenchyme in *Has2*^{cko} (Fig. 5E′, arrow), which is not evident in wildtype (Fig. 5D′, arrow), suggesting loss of tethering resulting in aberrant distribution of CSPG. This notion is in agreement with the fact that HA is required for CSPG assembly and retention in the ECM (Day, 1999; Hardingham, 1979; Knudson, 1993; Kochhar et al., 1984; Maleski and Knudson, 1996b; Morgelin et al., 1994, 1988; Seyfried et al., 2005).

Aggrecan is a high molecular mass HA-binding CSPG abundant in cartilage pericellular matrix and forms an aggregate network with HA (Day, 1999; Hardingham, 1979; Hardingham and Fosang, 1992; Lee et al., 1993; Morgelin et al., 1994, 1988). Immunolabeling for aggrecan was reduced in the condensing digits (Fig. 5F and G) but showed enhanced ectopic localization in the interdigital mesenchyme at E13.5 (Fig. 5F′ and G′, arrows). Similarly, link protein, which stabilizes HA-aggrecan aggregates in cartilage

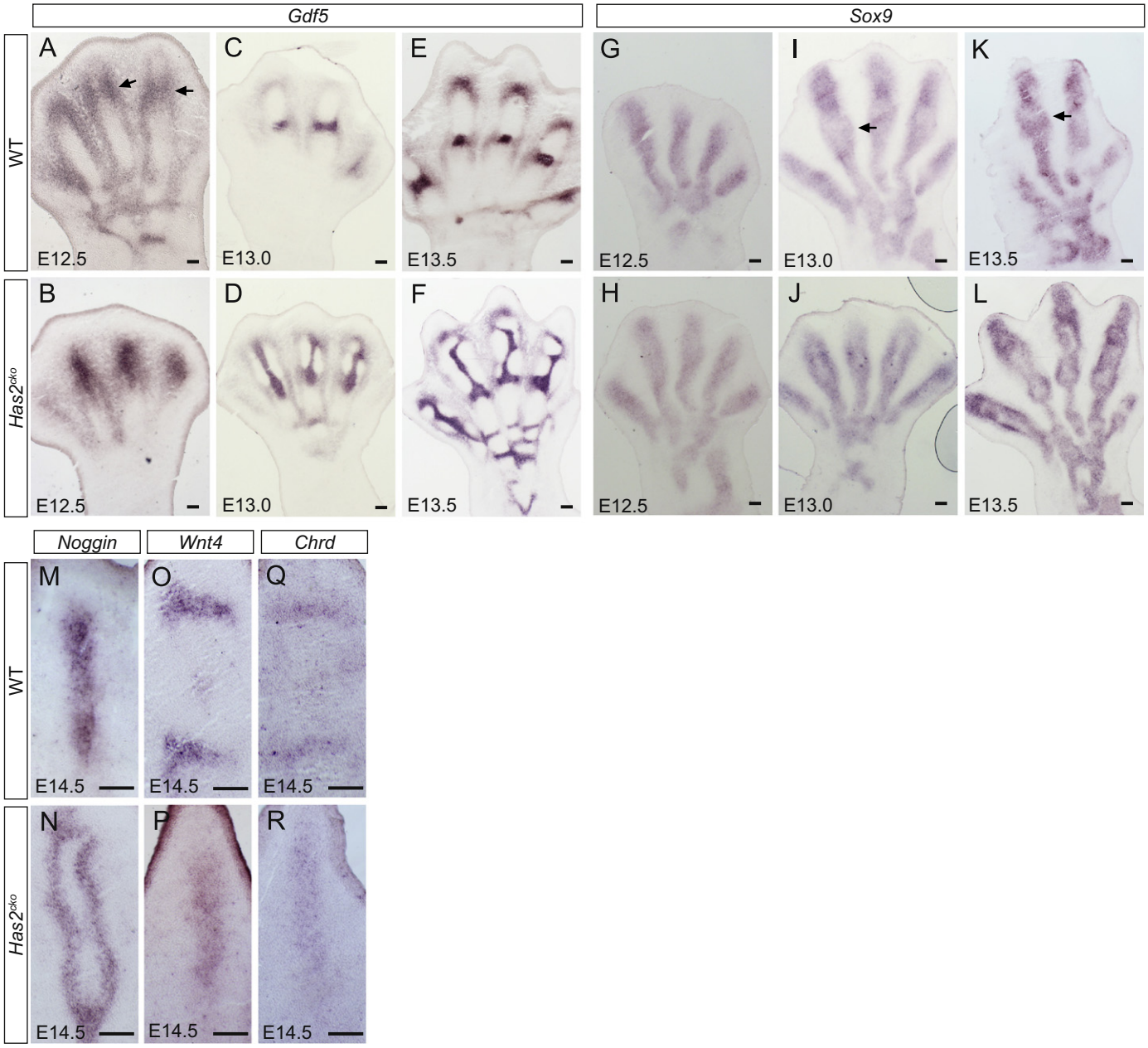

Fig. 4. Joint markers indicate aberrant positioning of the interzone in *Has2*^{cko}. Section in situ hybridization analysis for *Gdf5* (A–F) and *Sox9* (G–L) expression in wild-type (A, C, E, G, I and K) and *Has2*^{cko} (B, D, F, H, J and L) limbs. The joint defects in *Has2*^{cko} can be detected as early as E12.5 when *Gdf5* expression, which highlights the position of forming interzone (A, arrow), is expanded (B). The aberrant *Gdf5* expression becomes progressively more severe (C versus D) and by E13.5 the interzone is clearly orthogonally shifted in *Has2*^{cko} mutant limbs (E versus F). Similarly, *Sox9* expressions in the chondrocytic domain also highlight the defective interzone formation in *Has2*^{cko} (G–L). Arrows mark interzone where *Sox9* expression is absent, and this *Sox9* negative zone is expanded in *Has2*^{cko} digits. Similar to *Sox9*, *Noggin* expression is absent in the center of the condensing chondrocytes in *Has2*^{cko} digits but instead surrounds the orthogonally shifted joint (compare M and N). RNA in situ hybridization analyses showing ectopic expression of additional joint interzone markers, *Wnt4* and *Chordin*, in *Has2*^{cko} hindlimb digits (P and R) compared with wildtype (O and Q) at E14.5. Scale bar, 50 μm.

(Watanabe and Yamada, 1999), was strikingly reduced in condensing digits and distributed aberrantly in the interdigital mesenchyme of *Has2*^{cko} limbs (Fig. 5H, I and H′, I′, arrows). Collectively, these findings highlight a crucial role for HA in assembling the pericellular CSPG matrix for proper mesenchymal condensation and subsequent interzone positioning.

Discussion

Chondrogenic differentiation and joint patterning in the developing vertebrate limb are dependent on cell-matrix interactions. Previous studies suggested that inductive signals regulate limb bud subridge mesoderm to maintain a relatively high rate of HA synthesis (Knudson and Toole, 1988). Consistent with this, bFGF was subsequently shown to stimulate HA synthesis in cultured chick embryonic limb mesodermal cells (Munaim et al., 1991). Other in vitro studies also showed that *Hyaluronan synthase* (*Has*) expression can be regulated by growth factors and cytokines (Jiang et al., 2011). However, the signal that induces the expression of *Has* during limb development is not known. Our study reveals that the molecular control of *Has2* gene expression in the early developing limb is Shh signaling. We demonstrated by genetic and molecular analyses that Shh signaling directly

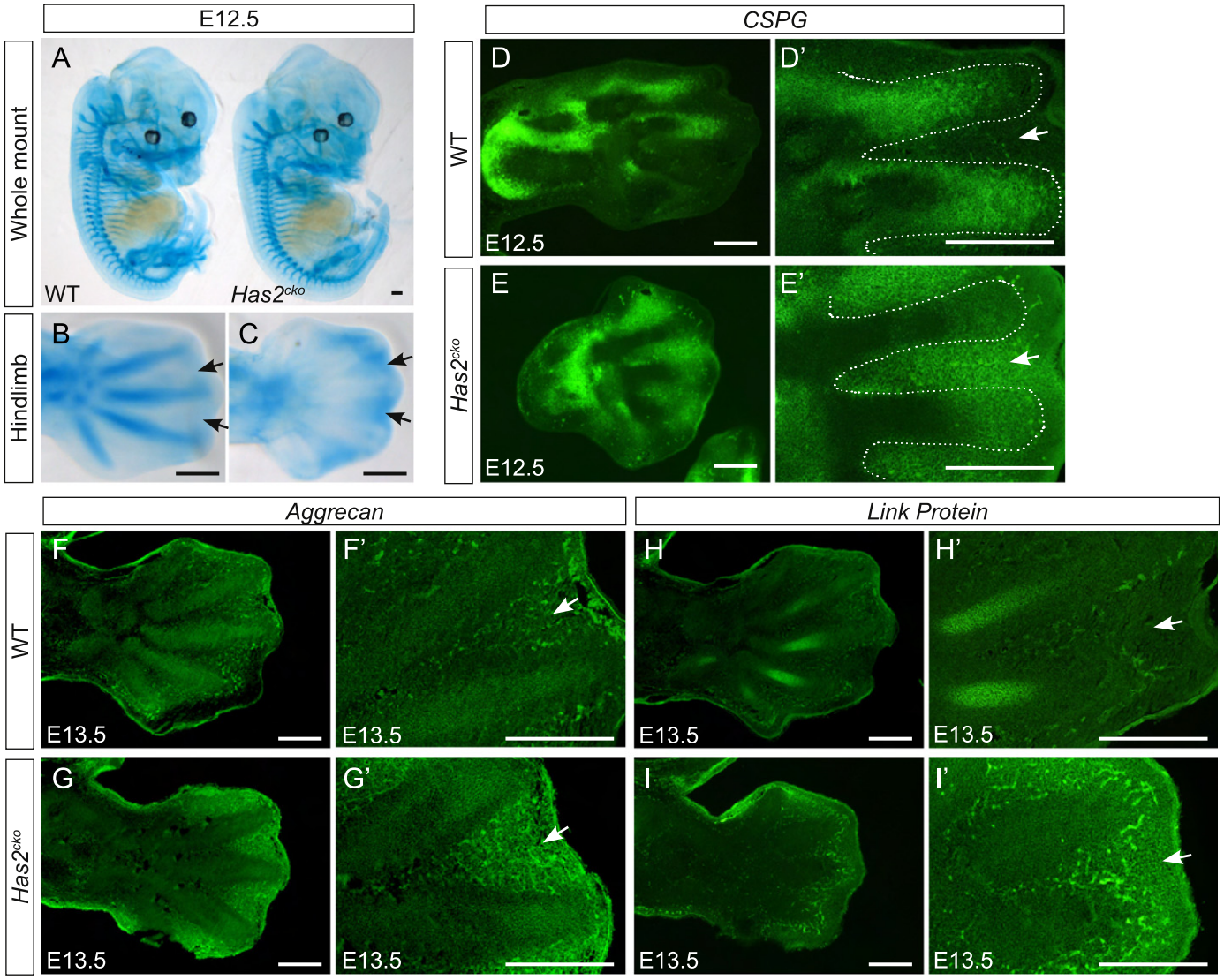

Fig. 5. Loss of *Has2* disrupts CSPG, aggrecan and link protein level and distribution. Alcian blue staining of sulfated proteoglycans in E12.5 wild-type and *Has2*^{cko} embryos. Whole-mount preparation showed comparable staining except in the hindlimb (A). This is better shown in higher magnification view in which *Has2*^{cko} digits lack intense Alcian blue staining seen in wildtype (B) but show striking acquisition of staining in the interdigital regions (arrows in C). Immunostaining of *Has2*^{cko} (E, E′, G, G′, I and I′) hindlimb sections compared with wild-type (D, D′, F, F′ H and H′) for total CSPG (D, D′, E and E′), aggrecan (F, F′, G G′ and D′) and link protein (H, H′, I and I′) showing markedly reduced expression of all these components, which normally form aggregates with HA, in *Has2*^{cko} hindlimb condensing digits (dotted line). CSPG is aberrantly distributed to the interdigital mesenchyme in *Has2*^{cko} limbs (compare arrow in D′ and E′), consistent with interdigital Alcian blue staining pattern in C, arrows. In contrast, CSPG is confined to condensing digits in wildtype with no apparent interdigital staining (arrow in D′). *Has2*^{cko} hindlimb buds also appear to have acquired interdigital staining for aggrecan (G′, arrow) and link protein (I′, arrow) which are confined to digits in wildtype. Scale bar, 150 μm.

regulates *Has2* expression during early limb development. While *Has2* expression in the posterior limb mesoderm is dependent on both positive Shh induction and Gli3R derepression, its expression in the anterior mesoderm is induced by Gli3R derepression. It is interesting to note that *Has2* expression seems to occur in two phases in the developing autopod; early Shh-induced *Has2* at E9.5–12.5 (Fig. 1) and a late-induced phase at around E14.5–E16.5, likely independent of Hh, in presumptive joints and perichondrium where Hh pathway is not activated (Dy et al., 2010). Because aberrant interzone development occurs as early as E12.5 (Fig. 4B), we propose that the regulation of *Has2* by Shh signaling is important in digit joint patterning. However, our study cannot rule out the contribution of late-phase *Has2* expression in joint development. We note that residual *Has2* expression still persists in *Shh* mutant limbs (Fig. 1), which may explain the relatively normal expression of *Gdf5* in the single un-ossified digit 1 (Chiang et al., 2001).

Our finding imparts new insights into the role of Shh signaling in HA extracellular matrix induction which functions in tissue injury and repair (Jiang et al., 2007), and has long been implicated in tumorigenicity (Adamia et al., 2005; Bourguignon, 2008; Toole and Hascall, 2002; Whatcott et al., 2011). Has/HA has been implicated in epithelial transformation, support of the cancer stem cell niche, regulating tumor-stromal interaction and growth and progression of a number of tumor types (Bernert et al., 2011; Bharadwaj et al., 2009; Kobayashi et al., 2010; Kosaki et al., 1999; Kramer et al., 2011; Li and Heldin, 2001; Li et al., 2007; Okuda et al., 2012; Paiva et al., 2005; Simpson, 2006; Simpson et al., 2001, 2002; Udabage et al., 2005; Zoltan-Jones et al., 2003). Our finding that Shh signaling induces *Has2*/HA expression can potentially be relevant in other developmental, injury or disease contexts where the Shh pathway is activated. Interestingly, *Rhamm* which encodes a hyaluronan-mediated motility receptor is also significantly upregulated in Shh pathway driven

medulloblastoma (Read et al., 2009). In addition, *Has2* is upregulated in microarrays from Shh-driven cerebellar tumors (Chiang, unpublished observation). It remains to be determined if *Has2* is a target of Shh signaling uniquely during limb development or in the broader context of Shh-driven pathologies where the stromal microenvironment and extracellular matrix play critical roles in disease progression.

Our finding underscores the essential role of Shh signaling in regulating the composition and function of the early limb ECM scaffold, a novel finding that stands in contrast to its known role in promoting cell proliferation. We generated *Has2* conditional mutants to determine the significance of Shh-induced *Has2* during limb development. A previous study had shown that *Has2* is required for chondrocyte maturation and joint formation (Matsumoto et al., 2009). Our study is consistent with their findings, but provides additional insights regarding the role of *Has2* in CSPG complex assembly and digit patterning. We found that our *Has2* mutants displayed a more severe phalangeal phenotype, with orthogonal shifting of digit interzones that progressively developed into joint cavities. This finding is strongly reminiscent of mutants that are defective in chondroitin sulfate synthesis or metabolism, and therefore underscores a central role of HA in the assembly of CSPG-aggregate complexes (see below). It is not entirely clear as to why our mutant phenotype is more severe than the previously reported *Has2* mutants. Because both alleles were designed to remove exon 2, it is unlikely that there are allele differences. One possibility is that we used $Has2^{fl/-}$ as opposed to $Has2^{fl/fl}$ (Matsumoto et al., 2009). Alternatively, there is evidence to suggest that the *Prx-cre* line does not efficiently excise target sequences when compared to the *Hoxb6-cre* line prior to E10.5 (Li et al., 2005; Scherz et al., 2007; Yu and Ornitz, 2008; Zhu et al., 2008).

The limb bud mesenchyme synthesizes CSPGs in prechondrogenic condensations (Hascall et al., 1976; Shinomura et al., 1984; Tsonis and Walker, 1991). We observed early changes in the pattern and expression of CSPG, aggrecan and link protein with significantly less labeling indicating reduced and diffuse deposition in $Has2^{cko}$ condensing digits. This finding is consistent with the role of HA in assembling the HA-CSPG network stabilized by link proteins (Day, 1999; Hardingham, 1979; Hardingham and Fosang, 1992; Kohda et al., 1996; Lee et al., 1993; Morgelin et al., 1994, 1988; Seyfried et al., 2005). Various HA perturbation studies in limb cultures suggested that HA promotes assembly and retention of CSPG for pericellular matrix organization and HA plays a role in cell–cell adhesion and interaction during mesenchymal condensation (Knudson, 1993; Knudson et al., 1999; Knudson and Toole, 1985; Kochhar et al., 1984; Maleski and Knudson, 1996a,b). Recent findings in vivo provide evidence for the essential role of CSPG and link protein in chondrogenesis. Mice deficient in CSPG biosynthesis developed skeletal dysplasia (Hiraoka et al., 2007). Abrogating *Chondroitin sulfate synthase* (*Chsy1*) or *Impad1*|*Jaws* resulted in impaired CSPG sulfation and defects in chondrocyte differentiation and maturation (Sohaskey et al., 2008; Wilson et al., 2012). Mutation of human *IMPAD1* leads to chondrodysplasia and joint abnormalities (Sohaskey et al., 2008; Vissers et al., 2011). Ablating link protein resulted in severe defects in chondrocyte organization, differentiation and maturation (Watanabe and Yamada, 1999). Indeed, our $Has2^{cko}$ limbs, with ectopic joints orthogonally shifted along the longitudinal axis, bear striking similarity to mutant limbs with impaired CSPG synthesis or sulfation (Sohaskey et al., 2008; Wilson et al., 2012), suggesting a central role of HA in the assembly of CSPG-aggregate complexes in vivo.

In addition to mutants that disrupt the composition of the ECM, inactivating *Hypoxia-inducible factor 1 α* (*Hif1α*) gene in the limb also produced longitudinal cavities representing aberrant joint patterning (Amarilio et al., 2007; Provot et al., 2007). However, the expression of the Hif1a target gene *Pgk1* or EF5 (a chemical probe for hypoxia) were not significantly changed in $Has2^{cko}$ limbs (Fig. S4). Together, these results suggest that the joint phenotype observed in $Has2^{cko}$ digits is not caused by changes in hypoxia regulation. While the precise mechanism by which *Has2* or CSPG deficiency leads to ectopic joint formation remains to be determined, it has been suggested that early *Gdf-5*-expressing cells migrate from the perichondrium region into the perimeter of developing cartilage (Pacifici et al., 2006; Storm and Kingsley, 1996). *Gdf5* is expressed in the perichondrium as well as interzone, and genetic fate mapping studies indicated that *Gdf5*-expressing cells contribute primarily to joint tissues including articular cartilage and synovial lining (Koyama et al., 2008). Given that *Gdf5* expression in the perichondrium is initiated normally in $Has2^{cko}$, it is possible that disruption of HA-CSPG complex in condensing prechondrocytes may permit aberrant migration and subsequent positioning of interzone precursor cells. In summary, we have established *Has2* as a direct downstream target of Shh signaling pathway and demonstrated that it is required for interzone positioning. Our finding underscores the essential role of Shh signaling in regulating the composition and function of the early limb ECM scaffold, a novel finding that stands in contrast to its known role in promoting cell proliferation.

Acknowledgments

Thanks to all Chiang lab members for suggestions throughout this study. The hypoxia marker EF5 was made available by the NCI and obtained through Dr. Cameron Koch at the University of Pennsylvania; we thank them for this valuable reagent. The Vanderbilt Transgenic Mouse/Embryonic Stem Cell Shared Resource helped with the injection of targeted ES cells. This work was funded by NIHRO1 HD49667 to C.C.

Supplemental method

EF5 staining

Pregnant females were i.p. injected with 10 mM EF5 (gift of NCI through Dr. Cameron Koch, University of Pennsylvania) in 5% dextrose and 2.4% ethanol, with an amount equal to 1/100 of the animal weight (1 ml/100g). Two hours after injection, embryos were collected and embedded in OCT freezing medium. Ten microgram frozen sections were collected and fixed in freshly prepared 4% PFA for 60 min. Slides were rinsed in PBST (PBS + 0.3% Tween 20) three times and blocked in PBST containing 2% milk and 5% goat serum at 4 °C overnight. Block solution was removed by dipping slides in PBST and stained for 6 h in 100 μl Alexa 488-conjugated ELK3-51 (anti-EF5) antibody solution (obtained from Dr. Cameron Koch). The slides were rinsed in PBST three times and mounted in FluorSave (Millipore, MA) for fluorescent imaging.

Appendix A. Supporting information

Supplementary data associated with this article can be found in the online version at http://dx.doi.org/10.1016/j.ydbio.2012.12.018.

References

Adamia, S., Maxwell, C.A., Pilarski, L.M., 2005. Hyaluronan and hyaluronan synthases: potential therapeutic targets in cancer. Curr. Drug Targets Cardiovasc. Haematol. Disord. 5, 3–14.

Ahrens, P.B., Solursh, M., Reiter, R.S., 1977. Stage-related capacity for limb chondrogenesis in cell culture. Dev. Biol. 60, 69–82.
Amarilio, R., Viukov, S.V., Sharir, A., Eshkar-Oren, I., Johnson, R.S., Zelzer, E., 2007. HIF1alpha regulation of Sox9 is necessary to maintain differentiation of hypoxic prechondrogenic cells during early skeletogenesis. Development 134, 3917–3928.
Bai, C.B., Stephen, D., Joyner, A.L., 2004. All mouse ventral spinal cord patterning by hedgehog is Gli dependent and involves an activator function of Gli3. Dev. Cell. 6, 103–115.
Bernert, B., Porsch, H., Heldin, P., 2011. Hyaluronan synthase 2 (HAS2) promotes breast cancer cell invasion by suppression of tissue metalloproteinase inhibitor 1 (TIMP-1). J. Biol. Chem. 286, 42349–42359.
Bharadwaj, A.G., Kovar, J.L., Loughman, E., Elowsky, C., Oakley, G.G., Simpson, M.A., 2009. Spontaneous metastasis of prostate cancer is promoted by excess hyaluronan synthesis and processing. Am. J. Pathol. 174, 1027–1036.
Bourguignon, L.Y., 2008. Hyaluronan-mediated CD44 activation of RhoGTPase signaling and cytoskeleton function promotes tumor progression. Semin. Cancer Biol. 18, 251–259.
Bowers, M., Eng, L., Lao, Z., Turnbull, R.K., Bao, X., Riedel, E., Mackem, S., Joyner, A.L., 2012. Limb anterior-posterior polarity integrates activator and repressor functions of GLI2 as well as GLI3. Dev Biol. 370, 110–124.
Camenisch, T.D., Spicer, A.P., Brehm-Gibson, T., Biesterfeldt, J., Augustine, M.L., Calabro Jr., A., Kubalak, S., Klewer, S.E., McDonald, J.A., 2000. Disruption of hyaluronan synthase-2 abrogates normal cardiac morphogenesis and hyaluronan-mediated transformation of epithelium to mesenchyme. J. Clin. Invest. 106, 349–360.
Cash, D.E., Bock, C.B., Schughart, K., Linney, E., Underhill, T.M., 1997. Retinoic acid receptor alpha function in vertebrate limb skeletogenesis: a modulator of chondrogenesis. J. Cell Biol. 136, 445–457.
Chiang, C., Litingtung, Y., Harris, M.P., Simandl, B.K., Li, Y., Beachy, P.A., Fallon, J.F., 2001. Manifestation of the limb prepattern: limb development in the absence of sonic hedgehog function. Dev. Biol. 236, 421–435.
Copeland, N.G., Jenkins, N.A., Court, D.L., 2001. Recombineering: a powerful new tool for mouse functional genomics. Nat. Rev. Genet. 2, 769–779.
Day, A.J., 1999. The structure and regulation of hyaluronan-binding proteins. Biochem. Soc. Trans. 27, 115–121.
Day, A.J., Prestwich, G.D., 2002. Hyaluronan-binding proteins: tying up the giant. J. Biol. Chem. 277, 4585–4588.
Dy, P., Smits, P., Silvester, A., Penzo-Mendez, A., Dumitriu, B., Han, Y., de la Motte, C.A., Kingsley, D.M., Lefebvre, V., 2010. Synovial joint morphogenesis requires the chondrogenic action of Sox5 and Sox6 in growth plate and articular cartilage. Dev. Biol. 341, 346–359.
Fernandez-Teran, M.A., Hinchliffe, J.R., Ros, M.A., 2006. Birth and death of cells in limb development: a mapping study. Dev. Dyn. 235, 2521–2537.
Gavin, B.J., McMahon, J.A., McMahon, A.P., 1990. Expression of multiple novel Wnt-1/int-1-related genes during fetal and adult mouse development. Genes Dev. 4, 2319–2332.
Hallikas, O., Palin, K., Sinjushina, N., Rautiainen, R., Partanen, J., Ukkonen, E., Taipale, J., 2006. Genome-wide prediction of mammalian enhancers based on analysis of transcription-factor binding affinity. Cell 124, 47–59.
Hardingham, T.E., 1979. The role of link-protein in the structure of cartilage proteoglycan aggregates. Biochem. J. 177, 237–247.
Hardingham, T.E., Fosang, A.J., 1992. Proteoglycans: many forms and many functions. FASEB J. 6, 861–870.
Hascall, V.C., Oegema, T.R., Brown, M., 1976. Isolation and characterization of proteoglycans from chick limb bud chondrocytes grown in vitro. J. Biol. Chem. 251, 3511–3519.
Hiraoka, S., Furuichi, T., Nishimura, G., Shibata, S., Yanagishita, M., Rimoin, D.L., Superti-Furga, A., Nikkels, P.G., Ogawa, M., Katsuyama, K., Toyoda, H., Kinoshita-Toyoda, A., Ishida, N., Isono, K., Sanai, Y., Cohn, D.H., Koseki, H., Ikegawa, S., 2007. Nucleotide-sugar transporter SLC35D1 is critical to chondroitin sulfate synthesis in cartilage and skeletal development in mouse and human. Nat. Med. 13, 1363–1367.
Huang, X., Liu, J., Ketova, T., Fleming, J.T., Grover, V.K., Cooper, M.K., Litingtung, Y., Chiang, C., 2010. Transventricular delivery of Sonic hedgehog is essential to cerebellar ventricular zone development. Proc. Natl. Acad. Sci. USA 107, 8422–8427.
James, C.G., Appleton, C.T., Ulici, V., Underhill, T.M., Beier, F., 2005. Microarray analyses of gene expression during chondrocyte differentiation identifies novel regulators of hypertrophy. Mol. Biol. Cell. 16, 5316–5333.
Jiang, D., Liang, J., Noble, P.W., 2007. Hyaluronan in tissue injury and repair. Annu. Rev. Cell. Dev. Biol. 23, 435–461.
Jiang, D., Liang, J., Noble, P.W., 2011. Hyaluronan as an immune regulator in human diseases. Physiol. Rev. 91, 221–264.
Khan, I.M., Redman, S.N., Williams, R., Dowthwaite, G.P., Oldfield, S.F., Archer, C.W., 2007. The development of synovial joints. Curr. Top. Dev. Biol. 79, 1–36.
Kinzler, K.W., Vogelstein, B., 1990. The GLI gene encodes a nuclear protein which binds specific sequences in the human genome. Mol. Cell. Biol. 10, 634–642.
Klingensmith, J., Ang, S.L., Bachiller, D., Rossant, J., 1999. Neural induction and patterning in the mouse in the absence of the node and its derivatives. Dev. Biol. 216, 535–549.
Knudson, C.B., 1993. Hyaluronan receptor-directed assembly of chondrocyte pericellular matrix. J. Cell. Biol. 120, 825–834.
Knudson, C.B., Nofal, G.A., Pamintuan, L., Aguiar, D.J., 1999. The chondrocyte pericellular matrix: a model for hyaluronan-mediated cell-matrix interactions. Biochem. Soc. Trans. 27, 142–147.
Knudson, C.B., Toole, B.P., 1985. Changes in the pericellular matrix during differentiation of limb bud mesoderm. Dev. Biol. 112, 308–318.
Knudson, C.B., Toole, B.P., 1988. Epithelial-mesenchymal interaction in the regulation of hyaluronate production during limb development. Biochem. Int. 17, 735–745.
Kobayashi, N., Miyoshi, S., Mikami, T., Koyama, H., Kitazawa, M., Takeoka, M., Sano, K., Amano, J., Isogai, Z., Niida, S., Oguri, K., Okayama, M., McDonald, J.A., Kimata, K., Taniguchi, S., Itano, N., 2010. Hyaluronan deficiency in tumor stroma impairs macrophage trafficking and tumor neovascularization. Cancer Res. 70, 7073–7083.
Kochhar, D.M., Penner, J.D., Hickey, T., 1984. Retinoic acid enhances the displacement of newly synthesized hyaluronate from cell layer to culture medium during early phases of chondrogenesis. Cell Differ. 14, 213–221.
Kohda, D., Morton, C.J., Parkar, A.A., Hatanaka, H., Inagaki, F.M., Campbell, I.D., Day, A.J., 1996. Solution structure of the link module: a hyaluronan-binding domain involved in extracellular matrix stability and cell migration. Cell 86, 767–775.
Kosaki, R., Watanabe, K., Yamaguchi, Y., 1999. Overproduction of hyaluronan by expression of the hyaluronan synthase Has2 enhances anchorage-independent growth and tumorigenicity. Cancer Res. 59, 1141–1145.
Koyama, E., Shibukawa, Y., Nagayama, M., Sugito, H., Young, B., Yuasa, T., Okabe, T., Ochiai, T., Kamiya, N., Rountree, R.B., Kingsley, D.M., Iwamoto, M., Enomoto-Iwamoto, M., Pacifici, M., 2008. A distinct cohort of progenitor cells participates in synovial joint and articular cartilage formation during mouse limb skeletogenesis. Dev. Biol. 316, 62–73.
Kramer, M.W., Escudero, D.O., Lokeshwar, S.D., Golshani, R., Ekwenna, O.O., Acosta, K., Merseburger, A.S., Soloway, M., Lokeshwar, V.B., 2011. Association of hyaluronic acid family members (HAS1, HAS2, and HYAL-1) with bladder cancer diagnosis and prognosis. Cancer 117, 1197–1209.
Lee, G.M., Johnstone, B., Jacobson, K., Caterson, B., 1993. The dynamic structure of the pericellular matrix on living cells. J. Cell. Biol. 123, 1899–1907.
Lee, J.Y., Spicer, A.P., 2000. Hyaluronan: a multifunctional, megaDalton, stealth molecule. Curr. Opin. Cell. Biol. 12, 581–586.
Lev, R., Spicer, S.S., 1964. Specific staining of sulphate groups with Alcian blue at low pH. J. Histochem. Cytochem. 12, 309.
Li, C., Xu, X., Nelson, D.K., Williams, T., Kuehn, M.R., Deng, C.X., 2005. FGFR1 function at the earliest stages of mouse limb development plays an indispensable role in subsequent autopod morphogenesis. Development 132, 4755–4764.
Li, Y., Gordon, J., Manley, N.R., Litingtung, Y., Chiang, C., 2008. Bmp4 is required for tracheal formation: a novel mouse model for tracheal agenesis. Dev. Biol. 322, 145–155.
Li, Y., Heldin, P., 2001. Hyaluronan production increases the malignant properties of mesothelioma cells. Br. J. Cancer 85, 600–607.
Li, Y., Li, L., Brown, T.J., Heldin, P., 2007. Silencing of hyaluronan synthase 2 suppresses the malignant phenotype of invasive breast cancer cells. Int. J. Cancer 120, 2557–2567.
Li, Y., Zhang, H., Choi, S.C., Litingtung, Y., Chiang, C., 2004. Sonic hedgehog signaling regulates Gli3 processing, mesenchymal proliferation, and differentiation during mouse lung organogenesis. Dev. Biol. 270, 214–231.
Li, Y., Zhang, H., Litingtung, Y., Chiang, C., 2006. Cholesterol modification restricts the spread of Shh gradient in the limb bud. Proc. Natl. Acad. Sci. USA 103, 6548–6553.
Litingtung, Y., Dahn, R.D., Li, Y., Fallon, J.F., Chiang, C., 2002. Shh and Gli3 are dispensable for limb skeleton formation but regulate digit number and identity. Nature 418, 979–983.
Liu, P., Jenkins, N.A., Copeland, N.G., 2003. A highly efficient recombineering-based method for generating conditional knockout mutations. Genome Res. 13, 476–484.
Logan, M., Martin, J.F., Nagy, A., Lobe, C., Olson, E.N., Tabin, C.J., 2002. Expression of Cre Recombinase in the developing mouse limb bud driven by a Prxl enhancer. Genesis 33, 77–80.
Lowe, L.A., Yamada, S., Kuehn, M.R., 2000. HoxB6-Cre transgenic mice express Cre recombinase in extra-embryonic mesoderm, in lateral plate and limb mesoderm and at the midbrain/hindbrain junction. Genesis 26, 118–120.
Maleski, M.P., Knudson, C.B., 1996a. Hyaluronan-mediated aggregation of limb bud mesenchyme and mesenchymal condensation during chondrogenesis. Exp. Cell. Res. 225, 55–66.
Maleski, M.P., Knudson, C.B., 1996b. Matrix accumulation and retention in embryonic cartilage and in vitro chondrogenesis. Connect. Tissue Res. 34, 75–86.
Matsumoto, K., Li, Y., Jakuba, C., Sugiyama, Y., Sayo, T., Okuno, M., Dealy, C.N., Toole, B.P., Takeda, J., Yamaguchi, Y., Kosher, R.A., 2009. Conditional inactivation of Has2 reveals a crucial role for hyaluronan in skeletal growth, patterning, chondrocyte maturation and joint formation in the developing limb. Development 136, 2825–2835.
McMahon, J.A., Takada, S., Zimmerman, L.B., Fan, C.M., Harland, R.M., McMahon, A.P., 1998. Noggin-mediated antagonism of BMP signaling is required for growth and patterning of the neural tube and somite. Genes Dev. 12, 1438–1452.
Morgelin, M., Heinegard, D., Engel, J., Paulsson, M., 1994. The cartilage proteoglycan aggregate: assembly through combined protein-carbohydrate and protein-protein interactions. Biophys. Chem. 50, 113–128.
Morgelin, M., Paulsson, M., Hardingham, T.E., Heinegard, D., Engel, J., 1988. Cartilage proteoglycans. Assembly with hyaluronate and link protein as studied by electron microscopy. Biochem. J. 253, 175–185.

Motoyama, J., Milenkovic, L., Iwama, M., Shikata, Y., Scott, M.P., Hui, C.C., 2003. Differential requirement for Gli2 and Gli3 in ventral neural cell fate specification. Dev. Biol. 259, 150–161.
Munaim, S.I., Klagsbrun, M., Toole, B.P., 1991. Hyaluronan-dependent pericellular coats of chick embryo limb mesodermal cells: induction by basic fibroblast growth factor. Dev. Biol. 143, 297–302.
Nagy, A., Rossant, J., Nagy, R., Abramow-Newerly, W., Roder, J.C., 1993. Derivation of completely cell culture-derived mice from early-passage embryonic stem cells. Proc. Natl. Acad. Sci. USA 90, 8424–8428.
Ng, L.J., Wheatley, S., Muscat, G.E., Conway-Campbell, J., Bowles, J., Wright, E., Bell, D.M., Tam, P.P., Cheah, K.S., Koopman, P., 1997. SOX9 binds DNA, activates transcription, and coexpresses with type II collagen during chondrogenesis in the mouse. Dev. Biol. 183, 108–121.
Niswander, L., Jeffrey, S., Martin, G.R., Tickle, C., 1994. A positive feedback loop coordinates growth and patterning in the vertebrate limb. Nature 371, 609–612.
Okuda, H., Kobayashi, A., Xia, B., Watabe, M., Pai, S.K., Hirota, S., Xing, F., Liu, W., Pandey, P.R., Fukuda, K., Modur, V., Ghosh, A., Wilber, A., Watabe, K., 2012. Hyaluronan synthase HAS2 promotes tumor progression in bone by stimulating the interaction of breast cancer stem-like cells with macrophages and stromal cells. Cancer Res. 72, 537–547.
Pacifici, M., Koyama, E., Shibukawa, Y., Wu, C., Tamamura, Y., Enomoto-Iwamoto, M., Iwamoto, M., 2006. Cellular and molecular mechanisms of synovial joint and articular cartilage formation. Ann. N. Y. Acad. Sci. 1068, 74–86.
Paiva, P., Van Damme, M.P., Tellbach, M., Jones, R.L., Jobling, T., Salamonsen, L.A., 2005. Expression patterns of hyaluronan, hyaluronan synthases and hyaluronidases indicate a role for hyaluronan in the progression of endometrial cancer. Gynecol. Oncol. 98, 193–202.
Pan, Y., Bai, C.B., Joyner, A.L., Wang, B., 2006. Sonic hedgehog signaling regulates Gli2 transcriptional activity by suppressing its processing and degradation. Mol. Cell. Biol. 26, 3365–3377.
Pitsillides, A.A., 2003. Identifying and characterizing the joint cavity-forming cell. Cell. Biochem. Funct. 21, 235–240.
Pitsillides, A.A., Ashhurst, D.E., 2008. A critical evaluation of specific aspects of joint development. Dev. Dyn. 237, 2284–2294.
Provot, S., Zinyk, D., Gunes, Y., Kathri, R., Le, Q., Kronenberg, H.M., Johnson, R.S., Longaker, M.T., Giaccia, A.J., Schipani, E., 2007. Hif-1alpha regulates differentiation of limb bud mesenchyme and joint development. J. Cell. Biol. 177, 451–464.
Read, T.A., Fogarty, M.P., Markant, S.L., McLendon, R.E., Wei, Z., Ellison, D.W., Febbo, P.G., Wechsler-Reya, R.J., 2009. Identification of CD15 as a marker for tumor-propagating cells in a mouse model of medulloblastoma. Cancer Cell. 15, 135–147.
Riddle, R.D., Johnson, R.L., Laufer, E., Tabin, C., 1993. Sonic hedgehog mediates the polarizing activity of the ZPA. Cell 75, 1401–1416.
Rodriguez, C.I., Buchholz, F., Galloway, J., Sequerra, R., Kasper, J., Ayala, R., Stewart, A.F., Dymecki, S.M., 2000. High-efficiency deleter mice show that FLPe is an alternative to Cre-loxP. Nat. Genet. 25, 139–140.
Scherz, P.J., McGlinn, E., Nissim, S., Tabin, C.J., 2007. Extended exposure to Sonic hedgehog is required for patterning the posterior digits of the vertebrate limb. Dev. Biol. 308, 343–354.
Seo, H.S., Serra, R., 2007. Deletion of Tgfbr2 in Prx1-cre expressing mesenchyme results in defects in development of the long bones and joints. Dev. Biol. 310, 304–316.
Seyfried, N.T., McVey, G.F., Almond, A., Mahoney, D.J., Dudhia, J., Day, A.J., 2005. Expression and purification of functionally active hyaluronan-binding domains from human cartilage link protein, aggrecan and versican: formation of ternary complexes with defined hyaluronan oligosaccharides. J. Biol. Chem. 280, 5435–5448.
Shinomura, T., Kimata, K., Oike, Y., Maeda, N., Yano, S., Suzuki, S., 1984. Appearance of distinct types of proteoglycan in a well-defined temporal and spatial pattern during early cartilage formation in the chick limb. Dev. Biol. 103, 211–220.
Simpson, M.A., 2006. Concurrent expression of hyaluronan biosynthetic and processing enzymes promotes growth and vascularization of prostate tumors in mice. Am. J. Pathol. 169, 247–257.
Simpson, M.A., Reiland, J., Burger, S.R., Furcht, L.T., Spicer, A.P., Oegema Jr., T.R., McCarthy, J.B., 2001. Hyaluronan synthase elevation in metastatic prostate carcinoma cells correlates with hyaluronan surface retention, a prerequisite for rapid adhesion to bone marrow endothelial cells. J. Biol. Chem. 276, 17949–17957.
Simpson, M.A., Wilson, C.M., McCarthy, J.B., 2002. Inhibition of prostate tumor cell hyaluronan synthesis impairs subcutaneous growth and vascularization in immunocompromised mice. Am. J. Pathol. 161, 849–857.
Sohaskey, M.L., Yu, J., Diaz, M.A., Plaas, A.H., Harland, R.M., 2008. JAWS coordinates chondrogenesis and synovial joint positioning. Development 135, 2215–2220.
Stanton, L.A., Sabari, S., Sampaio, A.V., Underhill, T.M., Beier, F., 2004. p38 MAP kinase signalling is required for hypertrophic chondrocyte differentiation. Biochem. J. 378, 53–62.
Storm, E.E., Kingsley, D.M., 1996. Joint patterning defects caused by single and double mutations in members of the bone morphogenetic protein (BMP) family. Development 122, 3969–3979.
Taipale, J., Chen, J.K., Cooper, M.K., Wang, B., Mann, R.K., Milenkovic, L., Scott, M.P., Beachy, P.A., 2000. Effects of oncogenic mutations in Smoothened and Patched can be reversed by cyclopamine. Nature 406, 1005–1009.
te Welscher, P., Zuniga, A., Kuijper, S., Drenth, T., Goedemans, H.J., Meijlink, F., Zeller, R., 2002. Progression of vertebrate limb development through SHH-mediated counteraction of GLI3. Science 298, 827–830.
Toole, B.P., 2004. Hyaluronan: from extracellular glue to pericellular cue. Nat. Rev. Cancer. 4, 528–539.
Toole, B.P., Hascall, V.C., 2002. Hyaluronan and tumor growth. Am. J. Pathol. 161, 745–747.
Towers, M., Wolpert, L., Tickle, C., 2011. Gradients of signalling in the developing limb. Curr. Opin. Cell. Biol. 24, 181–187.
Tsonis, P.A., Walker, E., 1991. Cell populations synthesizing cartilage proteoglycan core protein in the early chick limb bud. Biochem. Biophys. Res. Commun. 174, 688–695.
Turley, E.A., Noble, P.W., Bourguignon, L.Y., 2002. Signaling properties of hyaluronan receptors. J. Biol. Chem. 277, 4589–4592.
Udabage, L., Brownlee, G.R., Waltham, M., Blick, T., Walker, E.C., Heldin, P., Nilsson, S.K., Thompson, E.W., Brown, T.J., 2005. Antisense-mediated suppression of hyaluronan synthase 2 inhibits the tumorigenesis and progression of breast cancer. Cancer Res. 65, 6139–6150.
Vissers, L.E., Lausch, E., Unger, S., Campos-Xavier, A.B., Gilissen, C., Rossi, A., Del Rosario, M., Venselaar, H., Knoll, U., Nampoothiri, S., Nair, M., Spranger, J., Brunner, H.G., Bonafe, L., Veltman, J.A., Zabel, B., Superti-Furga, A., 2011. Chondrodysplasia and abnormal joint development associated with mutations in IMPAD1, encoding the Golgi-resident nucleotide phosphatase, gPAPP. Am. J. Hum. Genet. 88, 608–615.
Vokes, S.A., Ji, H., McCuine, S., Tenzen, T., Giles, S., Zhong, S., Longabaugh, W.J., Davidson, E.H., Wong, W.H., McMahon, A.P., 2007. Genomic characterization of Gli-activator targets in sonic hedgehog-mediated neural patterning. Development 134, 1977–1989.
Vokes, S.A., Ji, H., Wong, W.H., McMahon, A.P., 2008. A genome-scale analysis of the cis-regulatory circuitry underlying sonic hedgehog-mediated patterning of the mammalian limb. Genes Dev. 22, 2651–2663.
Vortkamp, A., Gessler, M., Grzeschik, K.H., 1995. Identification of optimized target sequences for the GLI3 zinc finger protein. DNA Cell. Biol. 14, 629–634.
Wang, B., Fallon, J.F., Beachy, P.A., 2000. Hedgehog-regulated processing of Gli3 produces an anterior/posterior repressor gradient in the developing vertebrate limb. Cell 100, 423–434.
Watanabe, H., Yamada, Y., 1999. Mice lacking link protein develop dwarfism and craniofacial abnormalities. Nat. Genet. 21, 225–229.
Whatcott, C.J., Han, H., Posner, R.G., Hostetter, G., Von Hoff, D.D., 2011. Targeting the tumor microenvironment in cancer: why hyaluronidase deserves a second look. Cancer Discovery 1, 291–296.
Wilson, D.G., Phamluong, K., Lin, W.Y., Barck, K., Carano, R.A., Diehl, L., Peterson, A.S., Martin, F., Solloway, M.J., 2012. Chondroitin sulfate synthase 1 (Chsy1) is required for bone development and digit patterning. Dev. Biol. 363, 413–425.
Yu, K., Ornitz, D.M., 2008. FGF signaling regulates mesenchymal differentiation and skeletal patterning along the limb bud proximodistal axis. Development 135, 483–491.
Zhu, J., Nakamura, E., Nguyen, M.T., Bao, X., Akiyama, H., Mackem, S., 2008. Uncoupling Sonic hedgehog control of pattern and expansion of the developing limb bud. Dev. Cell. 14, 624–632.
Zoltan-Jones, A., Huang, L., Ghatak, S., Toole, B.P., 2003. Elevated hyaluronan production induces mesenchymal and transformed properties in epithelial cells. J. Biol. Chem. 278, 45801–45810.